

Room temperature ferromagnetism in ITO and Ni doped ITO

Seelam Harinath Babu, Shaik Kaleemulla*

Thin Films Laboratory, Department of Physics, VIT University, Vellore 632014, Tamilnadu, India

*Corresponding author. Tel: (+91) 9003386732; E-mail: skaleemulla@gmail.com

Received: 30 December 2015, Revised: 20 February 2016 and Accepted: 10 June 2016

ABSTRACT

To fabricate spintronics devices with easy of processing we require reliable dilute magnetic semiconductors (DMS) at room temperature. Here we report the development of DMS material based on Indium tin oxide (ITO) with optimal tin concentration ($(\text{In}_{0.95}\text{Sn}_{0.05})_2\text{O}_3$). The ITO and Ni-doped ITO nanoparticles were synthesized in quartz tube under reduced pressure at elevated temperature. The stoichiometric samples were crystallized in cubic bixbyite structure with change in the unit cell volume with Ni doping and shown average particle size of 50 nm in electron micrographs. Estimated energy band gap of Ni-doped ITO is found to be 3.15 eV. The magnetic properties of materials revealed that optimal doping of Sn gives highest magnetization and further increase of doping with Ni^{2+} ions in In^{3+} sites lead to deterioration of ferromagnetism induced by Sn^{4+} . The observed ferromagnetism is attributed to the localized ferromagnetic exchange interactions induced by spin polarized electrons trapped in oxygen vacancies. The deterioration of ferromagnetism is attributed to excess anionic vacancies created by Ni doping and promotion of antiferromagnetic exchange with increase of Ni^{2+} ion concentration as evidenced from magnetic hysteresis loop at 100 K. Copyright © 2016 VBRI Press.

Keywords: Dilute magnetic semiconductors; nanoparticles; ferromagnetism; indium oxide.

Introduction

Development of best dilute magnetic semiconductor (DMS) materials are necessary to device spintronics devices in which both spin and charge of the electrons are exploited [1]. Sustainable DMS materials can be developed by doping compatible magnetic transition metal (TM) ions into conventional semiconductors [2]. For the past one-and-half decade many researchers developed DMS materials with various host semiconductor oxide materials such as ZnO, TiO_2 , CeO_2 , In_2O_3 and SnO_2 [3-9] as well as alloy type semiconductor [10]. Semiconductor oxide based DMS show ferromagnetism at and above room temperature whereas the alloy based semiconductor show at low temperature (~ 100 K). In addition, the oxide semiconductors are cost effective and easy to synthesize compared to their counterpart alloy based DMS. However, the induced ferrimagnetic strength in these materials, at room temperature, by transition metal doping is moderate and requires further improvement for spintronics applications. In this efforts we have developed many In_2O_3 based DMS materials in the past [11-14]. To further improve ferromagnetic strength in DMS materials based on transparent semiconductor oxide, we have chosen Indium tin oxide ($(\text{In}_{0.95}\text{Sn}_{0.05})_2\text{O}_3$) as a host material for the current study.

Indium tin oxide is a wide band gap, transparent conductive oxide (TCO) semiconductor with body centered cubic unit cell with lattice constant 10.11Å. ITO films are the most widely used materials due to its relatively high conductivity and high transmittance in the visible region of

the solar spectrum [15]. It is widely used in optoelectronics applications such as flat-panel displays, functional glasses, solar cells, light emitting diodes, etc., owing to their unique property of high optical transparency and high electrical conductivity [16-19]. Thus the development of ITO based magnetic semiconductor will give us a new material which has best magnetic, optical and electrical properties. However, in the literature few reports are available on magnetic properties of ITO films (with less Sn doping concentration) and transition metal ion doped ITO films prepared by various deposition techniques [20, 21]. But very few reports are available on synthesis and magnetic properties of undoped and transition metal doped indium-tin-oxide nanoparticles using simple, low cost technique solid state reaction. Hence we made an effort to study the development of ferromagnetism in ITO and TM-doped ITO nanoparticles. We choose Ni^{2+} as a substitution element for In^{3+} ions. Here we report synthesis of ITO with optimal Sn concentration $(\text{In}_{0.95}\text{Sn}_{0.05})_2\text{O}_3$ and transition metal doped ITO nanoparticles and their crystal structural, morphology, composition, lattice vibrational, optical and magnetic studies at room temperature. Our studies have revealed that $(\text{In}_{0.95}\text{Sn}_{0.05})_2\text{O}_3$ shows highest magnetization and further substitution of In^{3+} by Ni^{2+} lead to deterioration of ferromagnetism due to increase anionic vacancies and antiferromagnetic coupling induced by Ni-O interactions.

Experimental

Materials synthesis

Commercially available In_2O_3 (99.999%), SnO_2 (99.99%) and NiO (99.99%) precursor powders were procured from

Sigma-Aldrich (India) and were used as received. The nominal Indium tin oxide ($\text{In}_{0.95}\text{Sn}_{0.05}\text{O}_3$) and Ni-doped ITO ($\text{In}_{0.90}\text{Sn}_{0.05}\text{Ni}_{0.05}\text{O}_3$) powder samples were prepared by mixing stoichiometric molar ratio of In_2O_3 , SnO_2 and NiO precursors in Agate mortar and pestle. The mixture was ground for 16 hrs to make it homogeneous fine powder. The resultant fine powders were loaded into a one-end closed quartz tube with 1 cm diameter and 10 cm length. This precursor loaded quartz tube was further enclosed in a large diameter quartz tube (reaction chamber) with 2.5 cm diameter and 75 cm length. The outer enclosure has a provision for evacuation to remove the gases from the reaction chamber during the synthesis. During the synthesis the reaction chamber was maintained at 2×10^{-3} mbar pressure using rotary vane pump and is placed in horizontal tubular microprocessor controlled furnace. The furnace was heated at low ramping to reach 800°C and then soaked for 6 hours and was cooled back to room temperature.

Characterization methods

Crystallinity and structural properties of the as synthesized ITO and Ni-doped ITO powders were studied by X-ray diffraction technique (X-ray diffractometer D8 Advance, BRUKER) using Cu-K α radiation. The surface morphology of the powders was studied by field emission scanning electron microscopy (FE-SEM, Carl Zeiss, EVO MA 15) and the composition of the samples were studied by energy dispersive analysis of X-ray, called EDAX, (OXFORD instrument, INCA PentaFET-X3). Chemical bonding changes in the samples were characterized by FTIR spectroscopy (Shimadzu). Lattice vibrational properties of the samples were investigated by Raman scattering spectrograph (LABRAM HR 800) recorded at an excitation wavelength of 633 nm in back scattering mode, at room temperature. Optical properties of nanoparticles were studied through diffused reference spectroscopy (JASCO V-670). Magnetic properties of the samples were studied through magnetic field dependent magnetization (hysteresis) loops upto 0.5 T field at room temperature by calibrated vibrating sample magnetometer (Lake Shore - 7303). The magnetic hysteresis loops were measured at low temperatures after cooling the samples to the respective temperature under zero magnetic fields.

Results and discussion

Fig. 1 shows the X-ray diffraction profiles of ITO and Ni doped ITO along with precursor NiO powder samples. Both the synthesized samples show single phase cubic structure with no segregation of secondary phases such as SnO_2 or NiO. The XRD patterns conformed that the nickel oxide phases were not observed in in these powder samples. The XRD profiles confirm that both the NiO and SnO_2 were doped into the In_2O_3 lattice. Three prominent peaks were observed in the NiO XRD profile (bottom) at diffraction angles (2θ) 37.1° , 43.3° and 62.8° assigned to the (1 1 1), (2 0 0) and (2 2 0) crystal planes, respectively. Among the three peaks the (2 0 0) plane peak is prominent. The observed diffraction peaks were exactly coincided with cubic structure of NiO (JCPDS 47-1049). No new phases such as NiO_2 , Ni_2O_3 were observed in the XRD profile. Thus it suggests that the dopant NiO is free from other

nickel oxide phases. The middle corresponds to indium-tin-oxide (ITO). All the diffraction peaks were best indexed with (2 1 1), (2 2 2), (4 0 0), (4 1 1), (3 3 2), (4 3 1), (5 2 1), (4 4 0), (4 3 3), (6 1 1), (5 4 1), (6 2 2), (6 3 1), (4 4 4), (5 4 3), (6 4 0), (7 2 1), and (6 4 2) plane reflections. All the indexed peaks exactly coincided with the cubic structure of In_2O_3 (JCPDS No. #06-0416).

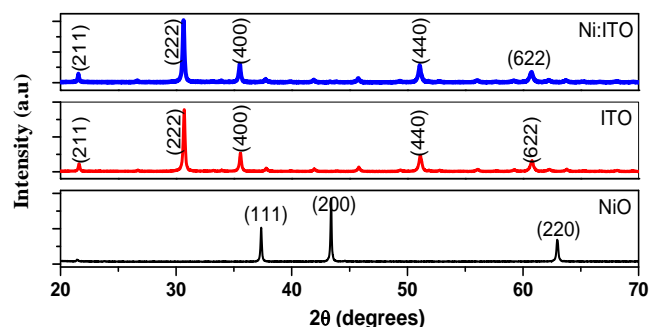


Fig. 1. X-ray diffraction profiles of NiO, ITO and Ni doped ITO nanoparticles.

The similar diffraction peaks were found in Ni doped ITO with small variation in diffraction angle [22]. No traces of secondary phases such as SnO_2 metal clusters of tin, nickel clusters, NiO and NiO_2 were found within the detection limit of XRD. A small shift in diffraction angle toward the lower angles was observed with introduction of Ni in ITO samples. It may be due to difference in the atomic radii of host and dopant elements. The ionic radius of indium ion (In^{+3} : 0.94 \AA) is larger than that of tin (Sn^{+4} : 0.83 \AA) and nickel (Ni^{+2} : 0.83 \AA). This indicates that both Ni and Sn ions were substituted into the In_2O_3 lattice rather than segregating as secondary phase. The crystallite size (G) was calculated by using the Debye-Scherrer formula [23],

$$G = k\lambda/\beta\cos\theta \quad (1)$$

where, k is crystallite geometry dependent constant and is 0.98 for spherical crystallites, λ is the wavelength of Cu K α ($\lambda = 1.5406 \text{ \AA}$), β is the full width at half maximum (FWHM) of diffraction peak at 2θ and θ is the diffracted angle, respectively. The estimated crystallite size using the above formula is found to be 47 nm for both undoped and Ni doped ITO nanoparticles. Generally, a decrease in the lattice parameter will be observed if the ionic radius of the dopant is smaller than the ionic radius of host element. In the present study, though the ionic radius of Ni^{2+} (0.83 \AA) is smaller than the ionic radius of In^{3+} (0.94 \AA) a decrease in the lattice parameter was not observed in Ni doped ITO samples.

Fig. 2 shows the surface morphology of the Ni doped ITO recorded through FE-SEM. The micrograph shows flocculated structure with elongated geometries. All the samples have shown contrast and it indicates that no secondary impurity phase existence. From the figure it is found that the average particle size of the powder was about 50 nm which is close to the crystallite size estimated from the X-ray diffraction profile.

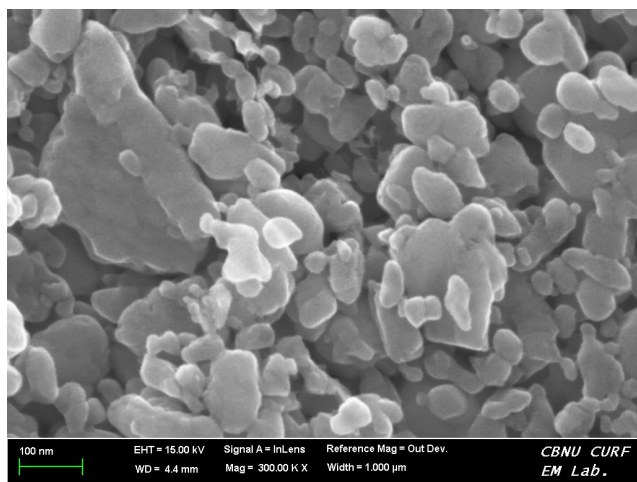


Fig. 2. FE-SEM image of Ni doped ITO nanoparticles.

This indicates that the particles have one grain and are single crystalline nature. To confirm the presence of metal ions as well as their distribution in the host lattice, $\kappa\alpha$ spectral imaging of sample was carried out using EDAX. Fig. 3 shows the EDAX spectrum of Ni doped ITO nanoparticles. The spectrum indicates the presence of indium, nickel, tin and oxygen elements at appropriate ratio with deficient oxygen. The estimated In, Sn, Ni and O atomic fractions are 35.18, 6.80, 1.04 and 51.70 at%, respectively. The data confirmed the doping of nickel into ITO lattice. For further confirmation, XPS study was also recorded to the ITO and Ni doped ITO nanoparticles.

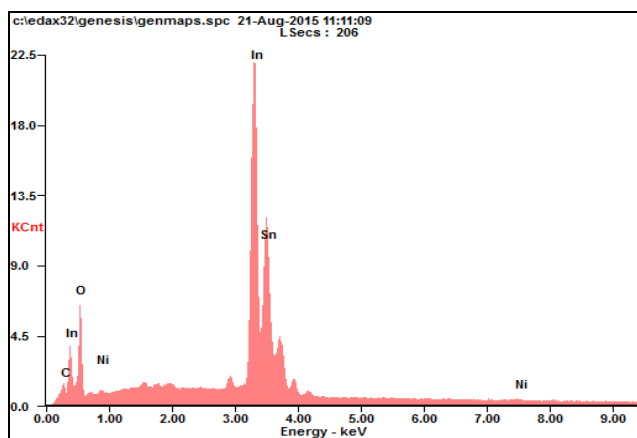


Fig. 3. EDAX spectrum of Ni doped ITO nanoparticles.

The FT-IR spectroscopic analysis was carried in order to study the bonding changes in Ni doped In_2O_3 samples. Fig. 4 shows the FT-IR spectra of ITO and Ni doped ITO nanoparticles. Many simple metal oxides with more than one oxygen atom bound to a single metal atom usually absorb in the region $1020 - 970 \text{ cm}^{-1}$ [24]. The Sn – O stretching vibrations are found in the region $800 - 300 \text{ cm}^{-1}$ [25]. The Sn – O stretching is usually observed around 670 and 560 cm^{-1} [26, 27]. In this present case, the Sn–O asymmetric and symmetric stretching vibrations appeared with very strong intensity at 617 and 520 cm^{-1} respectively in bulk phase whereas the same are observed at 630 and 530 cm^{-1} respectively in ITO nanoparticles.

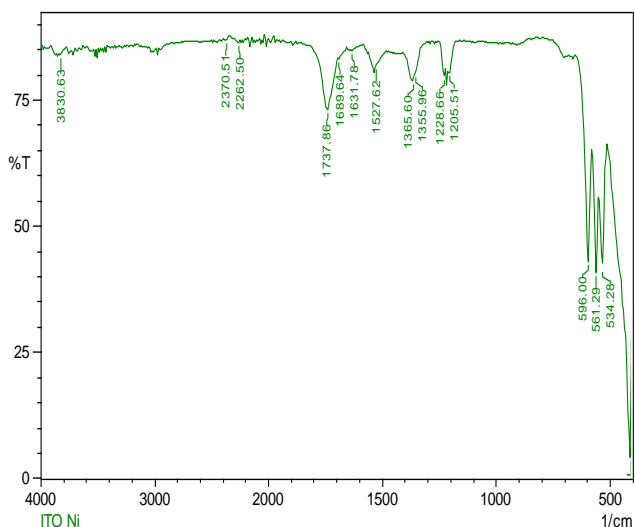
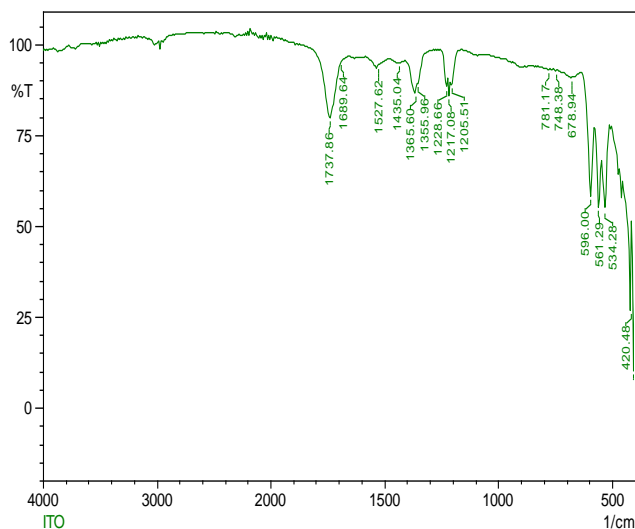


Fig. 4. FT-IR spectra of ITO and Ni doped ITO nanoparticles.

When compared with bulk, all the Sn – O vibrations are shifted towards higher energy of the spectra which is purely due to the change of bulk Sn–O to pseudo (super atoms) Sn–O as described by Rodumer *et al.* [28]. Absorption bands arising below the wavenumber 1000 cm^{-1} may be due to the stretching and bending vibrations predicted by a factor group analysis and lattice vibrations by Gerbier *et al.* [29] and additional peaks obtained above the wavenumber 1000 cm^{-1} could be due to the over tones. The cubic In_2O_3 powder had intense bands of the In – O stretching at the wavenumber of 440 cm^{-1} and 557 cm^{-1} . The FT-IR spectra of ITO and Ni doped ITO were almost similar in the appearance, however a small shift in the metal oxide bond peak was observed. As no new bands related to any other impurities were found, here it is inferred that Ni is doped in the ITO lattice.

Fig. 5 shows Raman spectra of In_2O_3 , SnO_2 , ITO and Ni doped ITO powders measured at room temperature. We have measured the unpolarized Raman spectra of Ni doped ITO samples to investigate the effects of the substitution of Sn and Ni ions in the In_2O_3 host lattice. From Fig. 5 it can be seen that the characteristic Raman peaks of In_2O_3 lying at $110, 132, 154, 164, 212, 249, 307, 365, 480, 495, 631 \text{ cm}^{-1}$ were in good agreement with the

results reported in the literature [30]. A small shift in Raman peaks were observed in case of ITO nanoparticles. They showed Raman peaks at 110, 131, 172, 214, 306, 365, 494, 629 cm^{-1} .

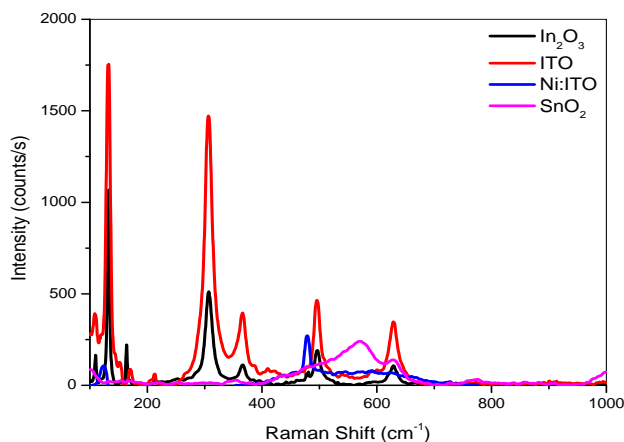


Fig. 5. Raman spectra of In_2O_3 , SnO_2 , ITO and Ni doped ITO samples.

Comparing doped samples, with pure In_2O_3 , we can see that the Raman spectra of these doped samples are almost identical to that of the pure sample, indicating that the (Sn, Ni) co-doped In_2O_3 nanoparticles retain good lattice order.

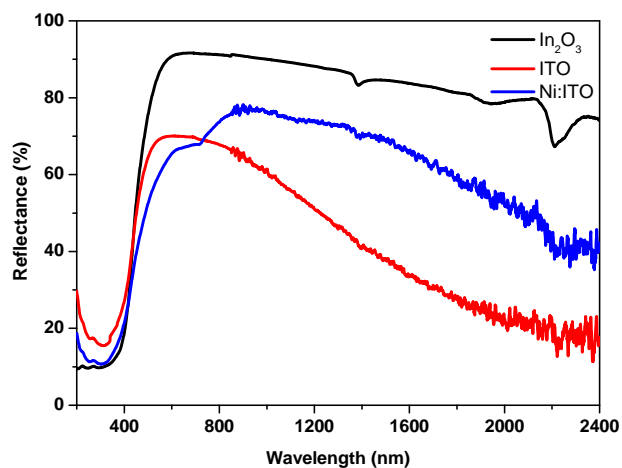


Fig. 6. The diffuse reflectance spectra of In_2O_3 , ITO and Ni doped ITO samples.

Fig. 6 shows the diffused reflectance spectra of the bulk In_2O_3 and nanosize ITO and Ni doped ITO nanoparticles recorded in the wavelength range from 200 nm to 2400 nm. The recorded optical reflectance was decreased for Ni doped ITO sample. In addition to reflectance spectra, absorption spectra were also estimated (not shown here) for calculating the optical band gap of the Ni doped ITO nanoparticles. The absorption coefficient was calculated using Kubelka-munk function [31] relation,

$$\alpha = (1-R)^2/2R \quad (2)$$

The optical band gap (E_g) was estimated by plotting $(\alpha h\nu)^2$ versus the photon energy ($h\nu$) and by extrapolating

the linear region ($\alpha = 0$). The optical band gap was estimated using the Tauc relation [32],

$$\alpha h\nu = A(E_g - h\nu)^{1/2} \quad (3)$$

An optical band gap of 3.15 eV was observed for Ni-doped ITO nanoparticles. The observed optical band gap is less than that of Ni doped In_2O_3 nanoparticles prepared by Ram prakash [33] and more than that of optical band gap of $\text{In}_{1.85}\text{Ni}_{0.15}\text{O}_3$ reported by Ahmed *et al.* [34].

The Fig. 7 shows magnetic hysteresis loops of ITO ($\text{In}_{1.95}\text{Sn}_{0.05}\text{Ni}_{0.05}\text{O}_3$) nanoparticles measured at room temperature under magnetic fields up to 5000 G which seems enough to saturate the magnetization in these samples. The hysteresis loops were also carried out for Ni doped In_2O_3 and Ni doped SnO_2 nanoparticles at room temperature [11, 14]. All the samples were shown ferromagnetism at room temperature with varied degree of magnetic strength. In addition, the precursor In_2O_3 and SnO_2 powders shown diamagnetic nature (data is not shown here). All the samples were synthesized from the same precursors with same conditions. Among all the Ni doped samples, Ni doped In_2O_3 shows high saturation mass magnetization than that of Ni doped SnO_2 whereas the Ni doped ITO powder did not shown noticeable ferromagnetism at room temperature. However, the Sn doped In_2O_3 sample shown highest saturation magnetization 0.05 emu/g.

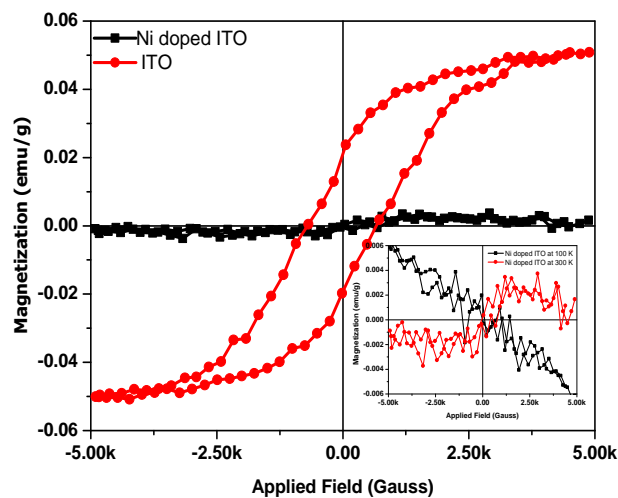


Fig. 7. M-H curve of ITO and Ni doped at 300 K.

All the samples were shown soft ferromagnetic nature with coercive fields around 100 G. As the precursor In_2O_3 and SnO_2 powder samples shown diamagnetic and their Ni-doped counterparts show ferromagnetism at room temperature, we infer that the ferromagnetism is induced by the substitution of In^{3+} by Ni^{2+} ions in the In_2O_3 . The observed saturation magnetization of $\text{In}_{1.95}\text{Ni}_{0.05}\text{O}_3$ is close to that of the $\text{In}_{1.95}\text{Ni}_{0.05}\text{O}_3$ powders prepared by solid state reaction [20]. In addition, Sn doped In_2O_3 (ITO) have shown much higher M_s than the Ni doped In_2O_3 . Hence we predicted that Ni doped ITO may show even higher magnetization (M_s) than ITO and thus we choose to dope optimal value of 2.5 at% of Ni into ITO. The bottom inset of the Fig. 7 shows magnetic hysteresis loop of Ni-doped ITO at temperature 300 and 100 K. It shows that with

decrease of temperature the ferromagnetism deteriorated further and become diamagnetic at 100 K. However, the results show that substitution of In^{3+} by Ni^{2+} ions in ITO lead to deterioration of ferromagnetism as seen in the **Fig. 7**. The deterioration may be due to present of different valency ions such as In^{3+} , Sn^{4+} and Ni^{2+} ions and antiferromagnetic exchange coupling between them. However, the following magnetic mechanism would be possible in the present ITO and Ni-doped ITO samples. Ferromagnetism may arise from magnetic exchange interactions between neighboring cations via “spin polarization electrons” trapped in anionic (oxygen) vacancies, called F-centered mediated ferromagnetism [35]. Such a mechanism is widely thought to be the most relevant to the origin of ferromagnetism in semiconductor oxide materials as well as oxide based DMS systems [36]. Such an intrinsic localized ferromagnetic exchange mechanism could also be possible in our ITO and Ni-doped ITO samples because there is no precipitation of secondary magnetic phases in our samples which could give rise to ferromagnetization. In addition, ferromagnetism in undoped semiconductor oxide also arises from oxygen vacancies in the lattice which are created during the synthesis. Such a vacancies will trap the single free electrons as explained by Coey *et al.* [35] and these trapped single electrons act as F-centers. The oxygen vacancies are most probable in our ITO and Ni-doped ITO samples due to synthesis of samples under vacuum conditions. In addition, oxygen vacancies will also arise when In^{3+} is substituted by lower valency ions such as Ni^{2+} and Co^{2+} in order to make charge compensation.

In ITO sample, both the host In^{3+} and doped Sn^{4+} ions have completely filled valency d-orbitals and hence predict diamagnetic nature of the sample. However, it shows ferromagnetic nature at room temperature and it may be due to oxygen vacancies mediated d^0 ferromagnetism as observed in vacuum annealed In_2O_3 films [37]. Such an oxygen vacancies mediated d^0 ferromagnetism also observed in SnO_2 [38] and HfO_2 [39] semiconductors. The deterioration of ferromagnetism in Ni-doped ITO may be attributed to the excessive oxygen defects present in the sample due to synthesis conditions as well as charge compensation requirement, as seen in the Bragg peak shift in **Fig. 1**. In addition, Ni doping may also favor antiferromagnetic exchange as in the NiO. Thus it could lead to deterioration of ferromagnetism and is also evidenced from magnetic hysteresis loop at 100 K as shown in inset of the **Fig. 7**.

Conclusion

Indium-tin-oxide (ITO) and Ni doped ITO nanoparticles were synthesized using simple solid state reaction and studied their structural, surface, chemical, optical and magnetic properties systematically. The undoped and Ni doped ITO nanoparticles exhibited cubic structure with about 47 nm crystallite size. A clear hysteresis loop has been observed for the ITO nanoparticles with magnetization 0.05 emu/g at room temperature. The strength of the magnetization decreased for the ITO nanoparticles at 100 K suggesting that ITO nanoparticles are best suited for room temperature ferromagnetism. However, the results showed that substitution of In^{3+} by

Ni^{2+} ions in ITO lead to deterioration of ferromagnetism. It suggests that impurity doped ITO nanoparticles are not suitable for the dilute magnetic semiconductors. The origin of room temperature ferromagnetism has been explained to the best of our knowledge.

Acknowledgements

Authors also thank VIT-SIF for providing XRD, Raman and UV-Vis-NIR facilities. The authors are highly thankful to Dr. R.K Kotnala, J. Dr. Shah and Dr. G.A. Bashheed, National Physical laboratory, India, for providing the vibrating sample magnetometer facilities.

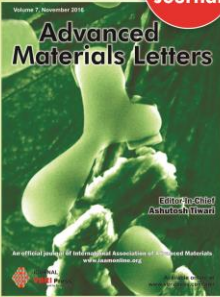
Author's contributions

Conceived the plan: SK; Performed the experiments: HB; Data analysis:SK; Wrote the paper: SK,HB. Authors have no competing financial interests.

References

1. Dietl, T.; Ohno, H.; Matsukura, F.; Cibert, J.; Ferrand, D. *Science*, **2000**, 287, 1019.
DOI: [10.1126/science.287.5455.1019](https://doi.org/10.1126/science.287.5455.1019).
2. Jonker, B.T.; Park, Y.D.; Bennett, B.R.; Cheong, H.D.; Kioseoglou, G.; Petrou, A. *Phys. Rev. B*, **2000**, 62, 8180.
DOI: [10.1103/PhysRevB.62.8180](https://doi.org/10.1103/PhysRevB.62.8180).
3. Kaushik, A.; Dalela, B.; Kumar, S.; Alvi, P.A.; Dalela, S. *Alloy Comp.* **2013**, 552, 274.
DOI: [10.1016/j.jallcom.2012.10.076](https://doi.org/10.1016/j.jallcom.2012.10.076).
4. Saleh, R.; Djaja, N.F.; Prakoso, S.P. *Alloy Comp.* **2013**, 546, 48.
DOI: [10.1016/j.jallcom.2012.08.056](https://doi.org/10.1016/j.jallcom.2012.08.056).
5. Jlaiel, F.; Amami, M.; Boudjida, N.; Strobel, P.; Salah, A.A.B. *Alloy Comp.* **2011**, 509, 7784.
DOI: [10.1016/j.jallcom.2011.04.153](https://doi.org/10.1016/j.jallcom.2011.04.153).
6. Khatoun, S.; Coolahan, K.; Lofland, S.E.; Ahmad, T. *Alloy Comp.* **2012**, 545, 162.
DOI: [10.1016/j.jallcom.2012.08.038](https://doi.org/10.1016/j.jallcom.2012.08.038).
7. Fitzgerald, C.B.; Venkatesan, M.; Douvalis, A.P.; Huber, S.; Coey, J. M. D.; Bakas, T. *J. Appl. Phys.* **2004**, 95, 7390.
DOI: [10.1063/1.1676026](https://doi.org/10.1063/1.1676026).
8. Ahmad, T.; Khatoun, S. *J. Mater. Res.* **2015**, 30, 1611.
DOI: [10.1557/jmr.2015.102](https://doi.org/10.1557/jmr.2015.102).
9. Khatoun, S.; Coolahan, K.; Lofland, S. E.; Ahmad, T. *J. Am. Ceram. Soc.* **2013**, 96, 2544.
DOI: [10.1111/jace.12361](https://doi.org/10.1111/jace.12361).
10. Ohno, H.; Shen, A.; Matsukura, F.; Oiwa, A.; Endo, A.; Katsumoto, S.; Iye, Y. *Appl. Phys. Lett.* **1996**, 69, 363.
DOI: [10.1063/1.118061](https://doi.org/10.1063/1.118061).
11. Krishna, N.S.; Kaleemulla, S.; Rao, N.M.; Kuppan, M.; Begam, M.R.; Reddy, D.S., *Mater. Sci. Semicon. Proc.* **2014**, 18, 22.
DOI: [10.1016/j.mssp.2013.10.012](https://doi.org/10.1016/j.mssp.2013.10.012).
12. Krishna, N.S.; Rao, N.M.; Kaleemulla, S.; Krishnamoorthi, C.; Begam, M.R.; Kuppan, M.; Reddy, D.S.; Omkaram, I. *Mater. Res. Bull.* **2015**, 61, 486.
DOI: [10.1016/j.materresbull.2014.10.065](https://doi.org/10.1016/j.materresbull.2014.10.065).
13. Kuppan, M.; Kaleemulla, S.; Rao, N.M.; Krishna, N.S.; Begam, M.R.; Reddy, D.S. *J. Supercond. Nov. Magn.* **2014**, 27, 1315.
DOI: [10.1007/s10948-013-2457-0](https://doi.org/10.1007/s10948-013-2457-0).
14. Kuppan, M.; Kaleemulla, S.; Krishna, N.S.; Rao, N.M.; Begam, M.R.; Shobana, M. *Adv. Cond. Matt. Phys.* **2014**, 1, 284237,
DOI: [10.1155/2014/284237](https://doi.org/10.1155/2014/284237).
15. Kim, H.M.; Bae, K.; Sohn, S. *Jpn. J. Appl. Phys.* **2011**, 50, 45801.
DOI: [10.1143/JJAP.50.045801](https://doi.org/10.1143/JJAP.50.045801).
16. Seo, J. W.; Park, J.W.; Lim, K. S.; Yang, J.H.; Kang, S. J. *Appl. Phys. Lett.* **2008**, 93, 223505.
DOI: [10.1063/1.3041643](https://doi.org/10.1063/1.3041643).
17. Han, H.; Mayer, J. W.; Alford, T. L. *J. Appl. Phys.* **2006**, 99, 123711.
DOI: [10.1063/1.2204815](https://doi.org/10.1063/1.2204815).
18. Han, H.; Adams, D.; Mayer, J.W.; Alford, T. L. *J. Appl. Phys.* **2005**, 98, 083705.
DOI: [10.1063/1.2106013](https://doi.org/10.1063/1.2106013).
19. Li, G.; Chu, C.W.; Shrotriya, V.; Huang, J.; Yang, Y. *Appl. Phys. Lett.* **2006**, 88, 253503
DOI: [10.1063/1.2212270](https://doi.org/10.1063/1.2212270).

20. Peleckis, G.; Wang, X.; Dou, S.X. *Appl. Phys. Lett.* **2006**, *89*,022501.
DOI: [10.1063/1.2220529](https://doi.org/10.1063/1.2220529)
21. Majumdar, H.S.; Majumdar, S.; Tobjörk, D.; Österbacka, R. *Syn. Metals.* **2010**, *160*, 303.
DOI: [10.1002/chin.201026204](https://doi.org/10.1002/chin.201026204)
22. Ay, F.; Aktaş, B.; Khaibullin, R.I.; Nuzhdin, V.I.; Rameev, B.Z. *J. Magn. Magn. Mater.* **2015**, *375*,129.
DOI: [10.1016/j.jmmm.2014.09.075](https://doi.org/10.1016/j.jmmm.2014.09.075)
23. Cullity, B.D. *Elements of X-ray Diffraction*, 2nd ed. Addison Wesley, Reading, MA, **1998**, 102.
24. Socrates G (Ed.) *Infrared and Raman Characteristics Group Frequencies*, third ed., Wiley, New York, **2001**.
25. Manjula, P.; Satyanarayana, L.; Swarnalatha, Y.; Manora, S.V. *Sens. Actuators B.* **2009**, *138*, 28.
DOI: [10.1016/j.snb.2009.02.051](https://doi.org/10.1016/j.snb.2009.02.051).
26. Yang, S.; Gao, L. *J. Am. Ceram. Soc.* **2006**, *89*, 1742.
DOI: [10.1111/j.1551-2916.2006.00947.x](https://doi.org/10.1111/j.1551-2916.2006.00947.x)
27. Popescu, D.A.; Verduraz, F.B. *Catal. Today.* **2001**, *70*, 139.
DOI: [10.1016/S0920-5861\(01\)00414-X](https://doi.org/10.1016/S0920-5861(01)00414-X)
28. Roduner, E. *Chem. Soc. Rev.* **2006**, *35*, 583.
DOI: [10.1039/B502142C](https://doi.org/10.1039/B502142C)
29. Gerbier, M.M.; Baraton, M.I.; Machet, J.; Quintard, P. *J. Mol. Struct.* **1984**, *115*,103.
DOI: [10.1016/0022-2860\(84\)80025-3](https://doi.org/10.1016/0022-2860(84)80025-3)
30. Dussan, S.; Singh, M.K.; Kumar, A.; Katiyar, S. *Int. Ferroelec.* **2011**, *125*,155.
DOI: [10.1080/10584587.2011.574483](https://doi.org/10.1080/10584587.2011.574483)
31. Lacombe, S.; Cardy, H.; Soggiu, N.; Blanc, S.; Jiawan, J.L.H.; Soumillion, J.P. *Micropor. Mesopor. Mater.* **2001**, *46*, 311.
DOI: [10.1016/S1387-1811\(01\)00315-8](https://doi.org/10.1016/S1387-1811(01)00315-8)
32. Tauc, J. *Amorphous and Liquid Semiconductors*, Plenum Press, **1974**, New York.
33. Prakash, R.; Kumar, S.; Ahmed, F.; Lee, C.G.; Song, J.I. *Thin Solid Films*, **2011**, *519*, 8243.
DOI: [10.1016/j.tsf.2011.03.105](https://doi.org/10.1016/j.tsf.2011.03.105)
34. Ahmad, T.; Khatoon, S.; Coolahan, K. *Mater Res Bull.* **2013**, *48*, 3065.
DOI: [10.1016/j.materresbull.2013.04.051](https://doi.org/10.1016/j.materresbull.2013.04.051)
35. J. M. D. Coey, A. P. Douvalis, C. B. Fitzgerald and M. Venkatesan, *Appl. Phys. Lett.* **2004**, *84*, 1332.
DOI: <http://dx.doi.org/10.1063/1.1650041>
36. Xing, P. F.; Chen, Y.X.; Yas, S. S.; Liu, G. L.; Mei, L. M.; Zhang, Z.; *J. Appl.Phys.* **2009**, *106*, 043909.
DOI: [10.1063/1.3202287](https://doi.org/10.1063/1.3202287)
37. Sun, S.; Wu, P.; Xing, P. J. *Magn. Magn. Mater.* **2012**, *324*, 2932.
DOI: [10.1016/j.jmmm.2012.04.050](https://doi.org/10.1016/j.jmmm.2012.04.050)
38. Rahman, G.; Suárez, V.M.G.; Hong, S.C. *Phys. Rev. B* **2008**, *78*, 184404.
DOI: [10.1103/PhysRevB.78.184404](https://doi.org/10.1103/PhysRevB.78.184404)
39. Chaitanya, D. P; Sanvito, S. *Phys. Rev. Lett.* **2005**, *94*, 217205.
DOI: [10.1103/PhysRevLett.94.217205](https://doi.org/10.1103/PhysRevLett.94.217205)



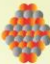
Volume 7, November 2016
Advanced Materials Letters
Editor-in-Chief: Ashutosh Tiwari

A Monthly Journal

Publish your article in this journal

Advanced Materials Letters is an official international journal of International Association of Advanced Materials (IAAM, www.iaamonline.org) published monthly by VBRI Press AB from Sweden. The journal is intended to provide high-quality peer-review articles in the fascinating field of materials science and technology particularly in the area of structure, synthesis and processing, characterisation, advanced-state properties and applications of materials. All published articles are indexed in various databases and are available download for free. The manuscript management system is completely electronic and has fast and fair peer-review process. The journal includes review article, research article, notes, letter to editor and short communications.

www.vbripress.com/aml



VBRI Press
Commitment to Excellence

Copyright © 2016 VBRI Press AB, Sweden